IL NUOVO CIMENTO **47 C** (2024) 22
DOI 10.1393/ncc/i2024-24022-3

Colloquia: COMEX7

Recent studies within the Subtracted Second RPA

D. Gambacurta
INFN, LNS - Catania, Italy

received 31 October 2023

Summary. — The Second Random Phase Approximation (SRPA) is an extension of the Random Phase Approximation (RPA) where more general excitation operators are introduced, including also two particle-two hole configurations, in addition to the one particle-one hole ones, already considered in the RPA. In the last years, systematic and large-scale SRPA calculations, without usually employed approximations have been performed. These calculations have shown severe limitation of the SRPA when effective interactions are employed, introducing double counting issues and instabilities. The SRPA model, upgraded by the subtraction method, designed to cure these difficulties, has been recently implemented and applied in the study of different physical cases. In this paper, we discuss some of the most recent results obtained by using this model, in particular concerning the dipole low-lying response and Gamow-Teller excitation in closed-shell nuclei.

1. – Introduction

The Random Phase Approximation (RPA) model provides a microscopic description of the nuclear collective excitations are build as superpositions of 1 particle-1 hole (1p1h) configurations. This approach is able to provide the global features of Giant Resonances (GR) such as the centroid energy, the total strength and the corresponding energy-weighted sum rules. However, it is not suited to describe other important properties as for example the GR's fine structure and the spreading width, generated by the coupling between 1p1h configurations with more complex degrees of freedom. The Second RPA (SRPA) model is a natural extension of RPA where a more general description of the nuclear excitations is considered and provides a valuable tool for the prediction of spreading widths and fine structure properties, due to the introduction of 2 particle-2 hole (2p2h) configurations. Only in the last years, large-scale SRPA calculations have been performed, showing merits and limits of this approach. Performing such calculations has allowed to show some features of the SRPA that could not be seen in previous applications, because of strong truncations in the model space or approximations. In particular, the SRPA spectrum is systematically lowered by several MeV with respect to the RPA [1-3], spoiling the typically good description obtained at RPA level.

The SRPA model has been recently improved by using the so-called subtraction procedure [4, 5] designed to handle the problem of the double counting of correlations when effective interactions are employed. This procedure cures some of the drawbacks and the limitations of the SRPA model providing thus a robust and stable theoretical tool for a beyond–mean–field description of the excitation spectra of many–body systems. In this work, we briefly report about some recent applications of the SRPA model based on the subtraction procedure.

2. – The subtraction procedure in SRPA

In the RPA approximation the excitations operators are assumed to be a linear superposition of 1p1h operators:

$$Q^{\dagger}_{\nu} = \sum_{ph} X^{\nu}_{ph} a^{\dagger}_{p} a_{h} - \sum_{ph} Y^{\nu}_{ph} a^{\dagger}_{h} a_{p}. \tag{1}$$

where for notation simplicity, the coupling to total quantum numbers is not indicated.

In the case of the SRPA, the 2p2h configurations are explicitly considered in the description of the excitations operators, having the following structure:

$$Q^{\dagger}_{\nu} = \sum_{ph} X^{\nu}_{ph} a^{\dagger}_{p} a_{h} - \sum_{ph} Y^{\nu}_{ph} a^{\dagger}_{h} a_{p}$$

$$+ \sum_{p<p',h<h'} (X^{\nu}_{php'h'} a^{\dagger}_{p'} a^{\dagger}_{p} a_{h'} a_{h} - Y^{\nu}_{php'h'} a^{\dagger}_{h} a^{\dagger}_{h'} a_{p} a_{p'}). \tag{2}$$

In both cases, the energies ω_ν of the excited states and their wave function (*e.g.*, the $X's$ and $Y's$ amplitudes) are obtained by solving an eigenvalue problem of this form:

$$\begin{pmatrix} \mathcal{A} & \mathcal{B} \\ -\mathcal{B}^{*} & -\mathcal{A}^{*} \end{pmatrix} \begin{pmatrix} \mathcal{X}^{\nu} \\ \mathcal{Y}^{\nu} \end{pmatrix} = \omega_{\nu} \begin{pmatrix} \mathcal{X}^{\nu} \\ \mathcal{Y}^{\nu} \end{pmatrix}. \tag{3}$$

In the RPA case the $\mathcal{A}$ and $\mathcal{B}$ matrices describe the coupling among the 1p1h configurations, while in SRPA, more general block matrices appear, describing the coupling of the 1p1h configurations with the 2p2h configurations and of the 2p2h configurations among themselves.

The subtraction procedure consists in subtracting in the A_{11} block of the SRPA matrix the quantity

$$E_{11'} = -\sum_{2,2'} A_{12} (A_{22'})^{-1} A_{2'1'} \tag{4}$$

where the indices 1 and 2 stand for the 1p1h and 2p2h configurations, respectively. This subtraction guarantees that the subtracted SRPA (SSRPA) response reduces to the RPA one in the zero–frequency limit. In the following sections, we show some applications of the SSRPA model. The SGII [6] interaction is employed in the following calculations.

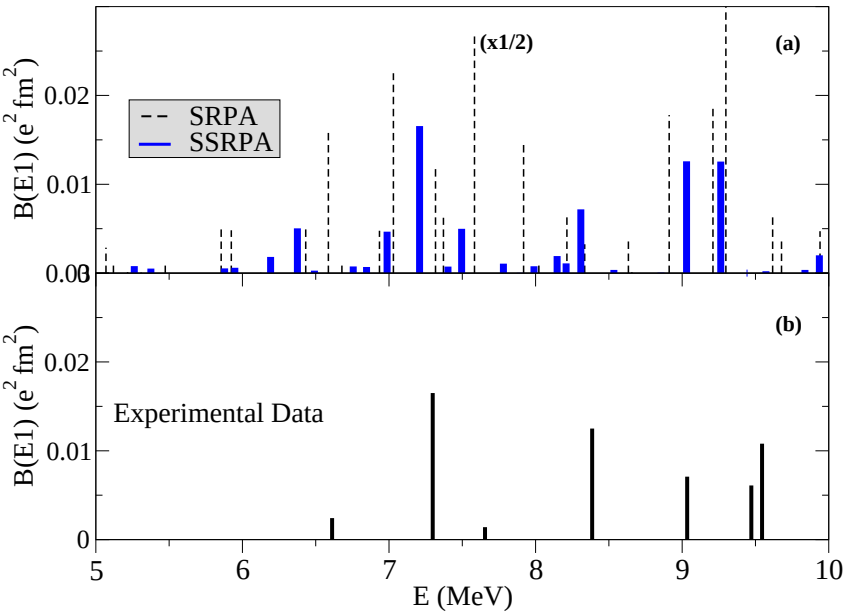

Fig. 1. – Low-lying dipole strength in ^{48}Ca: (a) Theoretical predictions for the transition probabilities $B(E1)$ calculated with the standard SRPA (dashed red bars; the values have been divided by 2) and with the SSRPA (blue thick bars); (b) Experimental $B(E1)$ values [7].

3. – Low-lying dipole response in ^{48}Ca and ^{68}Ni

The low–energy strength of dipole excitation spectra in neutron–rich nuclei is often referred as 'pygmy' because of its lower energy location and of its smaller contribution to the Energy weighted Sum Rule (EWSR) compared to Giant Dipole Resonance (GDR). In several cases, as indicated by the associated transition densities, such a strength is interpreted as produced by oscillations of the neutron skin of the nucleus against its core.

We start considering the dipole response below the neutron threshold in ^{48}Ca that has been measured with the (γ, γ') reaction [7]. The experimental data are shown in the lower panel of fig. 1. We recall here that, both relativistic and non-relativistic RPA predictions fail in reproducing such a low-lying strength either because the lowest RPA energies are larger than 10 MeV or because the RPA model cannot provide the observed fragmentation. A fragmented SRPA dipole strength below 10 MeV is instead found, as it can be seen from the upper panel of fig. 1 (black-dashed lines). However, the SRPA $B(E1)$ transition probability, integrated up to 10 MeV is considerably larger than the experimental value. In the same panel, the SSRPA results (blue lines) show that the subtraction procedure allows to achieve a strong improvement with respect to the SRPA, providing thus a rather good description of the experimental data. More precisely, the experimental $\sum B(E1)$ in (e^2 fm^2) and $\sum_i E_i B_i(E1)$ in (MeV e^2 fm^2) summed between 5 and 10 MeV are 0.068 $\pm$ 0.008 and 0.570 $\pm$ 0.062, respectively. The corresponding

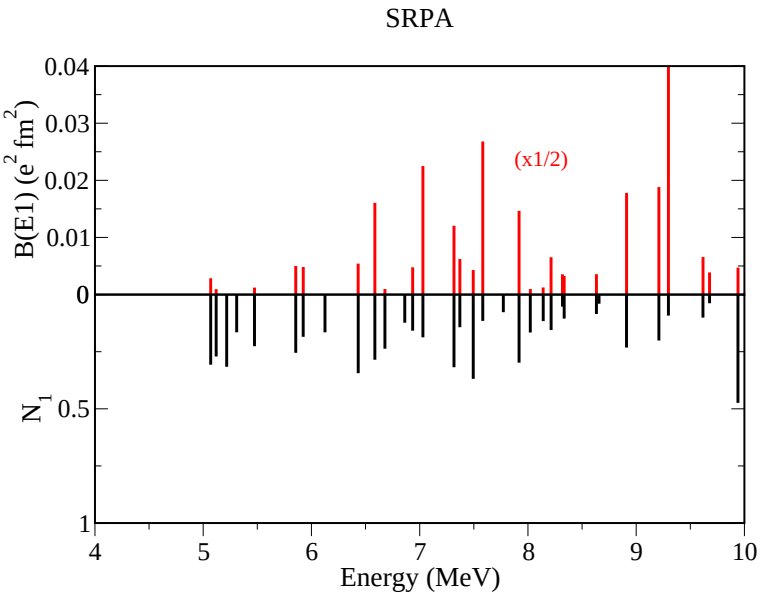

Fig. 2. – For each state the SRPA $B(E1)$ value and the total 1p1h contribution N_1 to the norm of the state defined in eq. (5) (lower panel), are shown.

values obtained in SRPA are 0.563 and 4.618, confirming the strong overestimation with respect to data. In the SSRPA case, we obtain instead 0.078 and 0.621, clearly showing the strong improvement.

A deeper insight on the properties of the excited states can be obtained by looking at their composition in terms of 1p1h and 2p2h configurations. The amount of 1p1h (2p2h) component can be evaluated by considering in the normalization of each state

$$(5) \qquad \sum_{ph}(\mid X^{\nu}_{ph} \mid^2 - \mid Y^{\nu}_{ph} \mid^2) + \sum_{p<p',h<h'} (\mid X^{\nu}_{php'h'} \mid^2 - \mid Y^{\nu}_{php'h'} \mid^2) = N_1 + N_2 = 1,$$

the N_1 (N_2) values. In figs. 2 and 3 we plot for each excited state (upper panels) the corresponding N_1 values (lower panels), obtained in SRPA and SSRPA, respectively. One can see that, in the SRPA case, a strong mixing of 1p1h and 2p2h components is found while, in the SSRPA case, states having mainly a 2p2h nature (as a consequence of the subtraction procedure), pushing up state with a strong 1p1h component.

We move now to the case of ^{68}Ni whose low–lying dipole strength was measured for the first time through virtual photon scattering at 600 MeV/nucleon at GSI [8]. A significant amount of strength (5% of the EWSR) was found to be centered at around 11 MeV. A second measurement was performed later, via relativistic Coulomb excitations, to extract the electric dipole polarizability [9]. A slightly different result was found this time, with a centroid located at 9.55 MeV and a contribution of 2.8% to the EWSR. The discrepancy

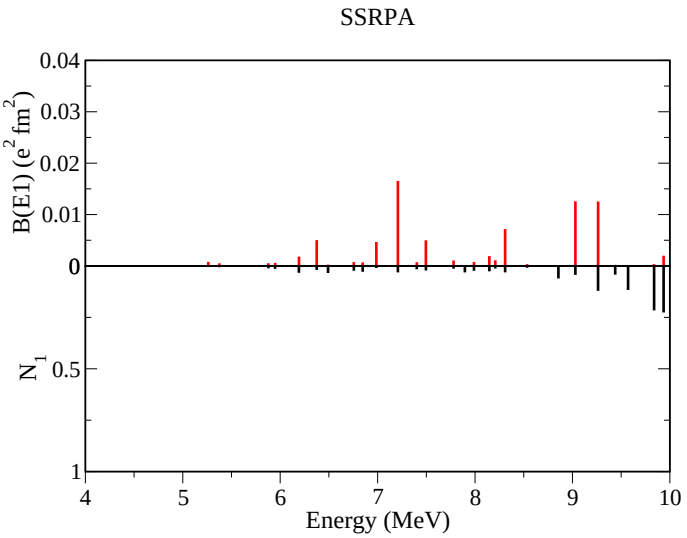

Fig. 3. – For each state the SSRPA $B(E1)$ value and the total 1p1h contribution N_1 to the norm of the state defined in eq. (5) (lower panel), are shown.

in the value of the centroid was explained as a possible 'energy–dependent branching ratio'. More recently [10], the first measurement done on ^{68}Ni using an hadronic probe (isoscalar ^{12}C target) waas performed at INFN-LNS in Catania. They found a centroid placed at around 10 MeV and a contribution of 9% to the EWSR.

In fig. 4, we compare the RPA and SSRPA spectra, upper and lower panel, respectively. We can see that the SSRPA spectrum is much denser compared to the RPA case, describing the physical fragmentation and fine structure. Focusing on the region below $\sim$ 12 MeV, we observe that there is more strength in the SSRPA spectrum which results in a higher percentage of EWSR in the low-energy region. This can be traced back to the inclusion of the 2p2h excitations. We also observe that the SSRPA low–energy distribution shows peaks concentrated around 9 and 10 MeV, as well as several peaks located just above 11 MeV, meaning that a significant amount of strength is predicted by the SSRPA model in the regions where the three experimental centroids are located. On the other side, in the low–energy part of the RPA spectrum there are much less peaks, the highest one being located between 9.5 and 10 MeV. Another isolated peak is placed below 11 MeV and there is practically no strength above 11 MeV. We may conclude that in SSRPA a larger fragmentation of the strength is found providing a better coverage of the region where the three experimental centroids were found.

In order to have a deeper understanding of the properties of the low-lying states, we plot, in figs. 5 and 6 the transition densities of the most collective states below 12 MeV. We see that the lowest states show neutron and proton transition densities having the typical features of a pygmy resonance, *e.g.*, dominant neutron contribution located at the surface of the nucleus, while the states at higher energy show a different behavior, being them most likely corresponding at the tail of GDR.

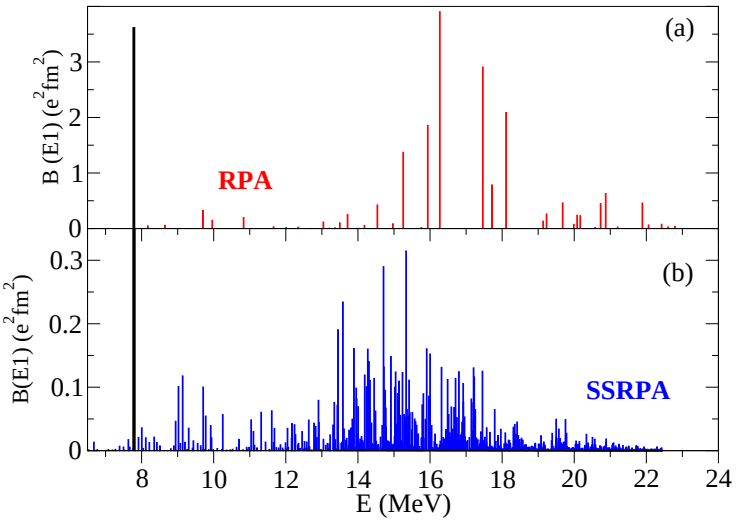

Fig. 4. – (a) RPA and (b) SSRPA dipole strength distribution obtained for ^{68}Ni. The vertical black line represents the neutron threshold.

4. – Gamow-Teller strength in ^{48}Ca

We then consider the Gamow-Teller(GT) strength in ^{48}Ca. It is very well known that, theoretical predictions of the GT strength usually overestimate the experimental data extracted by β-decay half-lives and one must resort to *ad hoc* "quenching factors" to obtain reasonable results for GT strength. This kind of over-prediction is usually ascribed to missing physics, for example the Δ excitation or complex configurations such as two-particle – two-hole excitations or two-body weak currents.

The strength functions are evaluated by using the GT one-body transition operators

$$\hat{O}^{\pm} = \sum_{i=1}^{A} \sum_{\mu} \sigma_{\mu}(i)\tau^{\pm}(i), \tag{6}$$

where $\tau^{\pm}$ are the isospin raising (+) and lowering (−) operators, $\tau^{\pm} = t_x \pm i t_y$, σ_μ is the spin operator, and A is the number of nucleons.

The $\hat{O}^{+}$ ($\hat{O}^{-}$) operator generates the GT^{+} (GT^{-}) strength where a neutron (proton) is added and a proton (neutron) is removed. The non-energy-weighted Ikeda sum rule [11], relates the integrated strengths S of the GT^{-} and the GT^{+} spectra to the difference of the number of neutrons N and protons Z reads as

$$S_{GT^-} - S_{GT^+} = 3(N - Z). \tag{7}$$

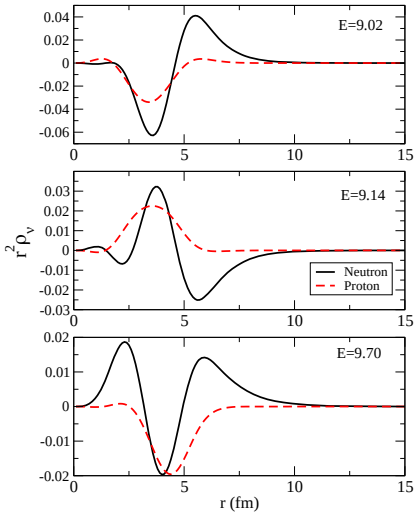

Fig. 5. – (Color online) Neutron and proton transition densities for the state located at different energies. The transition densities are multiplied by r^2 and are thus expressed in units of (fm^{-1}).

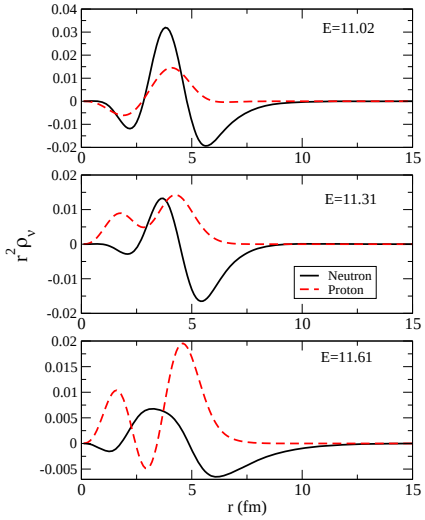

Fig. 6. – (Color online) Neutron and proton transition densities for the state located at different energies. The transition densities are multiplied by r^2 and are thus expressed in units of (fm^{-1}).

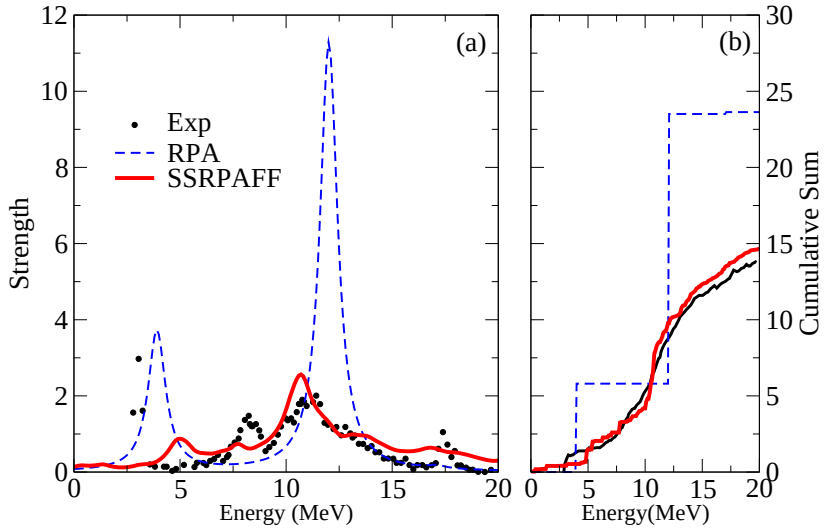

Fig. 7. – (a) GT^- strength distributions for the nucleus ^{48}Ca obtained with the SGII Skyrme interaction in MeV^{-1} compared with the experimental data [12]. RPA and all SSRPA strengths are obtained by folding with a Lorentzian having a width of 1 MeV. (b) Cumulative sum of the strength up to the excitation energy of 20 MeV. The excitation energy is referred with respect to the mother nucleus.

In fig. 7, we show the comparison of the RPA and SSRPA results, and how they compare with the experimental data [12]. In panel (a), the strength function is plotted, while in panel (b) the cumulative strengths up to 20 MeV is shown. It is clear how the SSRPA model is able to reproduce the fragmentation and spreading of the GT strength, while in RPA only two states absorb the full strength. This is especially clear in the displayed cumulative sums shown in the panel (b). Indeed, as it has been recently shown [13], this result is very weakly dependent on the employed parameterization and it is a genuine effect of the inclusion of the 2p2h configurations in the description of the excited states. We also note that, the experimental low-energy peak located at around 4 MeV, which is nicely described in RPA, in SSRPA is described by a broader distribution. However, as it can be seen in the right panel, the experimental and SSRPA cumulative strength are equal at around 5 MeV, suggesting that the strength is only fragmented over many states.

5. – Conclusions

We have shown and discussed recent applications of the SSRPA. As a first case, we studied the low-lying dipole response in ^{48}Ca, which can not be described by the standard RPA, and we show that the SSRPA results are in excellent agreement with experimental data. In the same section, we consider also the dipole strength distribution

of the unstable nucleus ^{68}Ni. The low–energy response is compared with three available experimental measurements, which led to the experimental centroids of 11 [8], 9.55 [9], and 10 [10] MeV. The SSRPA model provides peaks around these three energy values. Transition densities of most collective states show also the typical pygmy-like behavior.

We consider then the GT strength in ^{48}Ca, showing that the SSRPA strength below 20 MeV is much smaller than in RPA and in better agreement with the corresponding experimental values, without the use of any *ad hoc* quenching factors. This result is a strong merit ot the SSRPA, the key ingredient being the explicit inclusion of 2p2h configurations. Their density strongly increases with the excitation energy, leading to a high-energy tail in the spectrum.

REFERENCES

[1] Gambacurta D., Grasso M. and Catara F., *Phys. Rev. C*, **81** (2010) 054312.
[2] Gambacurta D., Grasso M. and Catara F., *Phys. Rev. C*, **84** (2011) 034301.
[3] Gambacurta D. *et al.*, *Phys. Rev. C*, **86** (2012) 021304(R).
[4] Gambacurta D., Grasso M. and Engel J., *Phys. Rev. C*, **92** (2015) 034303.
[5] Gambacurta D. and Grasso M., *Eur. Phys. J. A*, **52** (2016) 198.
[6] Giai N. V. and Sagawa H., *Phys. Lett. B*, **106** (1981) 379.
[7] Hartmann T. *et al.*, *Phys. Rev. Lett.*, **93** (2004) 192501.
[8] Wieland O. *et al.*, *Phys. Rev. Lett.*, **102** (2009) 092502.
[9] Rossi D. M. *et al.*, *Phys. Rev. Lett.*, **111** (2013) 242503.
[10] Martorana N. S. *et al.*, *Phys. Lett. B*, **782** (2018) 112.
[11] Ikeda K., Fuji S. and Fujita J., *Phys. Lett.*, **3** (1963) 271.
[12] Yako K. *et al.*, *Phys. Rev. Lett.*, **103** (2009) 012503.
[13] Gambacurta D., Grasso M. and Engel J., *Phys. Rev. Lett.*, **125** (2020) 212501.